*Progress In Electromagnetics Research M, Vol. 28, 27–39, 2013*

# AMPLITUDE-ONLY MEASUREMENTS OF A DUAL OPEN ENDED COAXIAL SENSOR SYSTEM FOR DETERMINATION OF COMPLEX PERMITTIVITY OF MATERIALS

**Kim Yee Lee[1, *], Boon Kuan Chung[1], Zulkifly Abbas[2], Kok Yeow You[3], and Ee Meng Cheng[4]**

[1]Centre for Communication Systems and Networks, Universiti Tunku Abdul Rahman, Kuala Lumpur 53300, Malaysia

[2]Department of Physics, Universiti Putra Malaysia, UPM Serdang 43300, Malaysia

[3]Department of Radio Communication Engineering, Universiti Teknologi Malaysia, UTM, Skudai, Johor 81310, Malaysia

[4]School of Mechatronic Engineering, University Malaysia Perlis, Ulu Pauh Campus, Arau, Perlis 02600, Malaysia

**Abstract**—This paper describes a novel permittivity measurement technique using dual open ended coaxial sensors. The magnitudes of the reflection coefficient from two open ended coaxial sensors were used to determine complex reflection coefficients and permittivity of a sample under test.

## 1. INTRODUCTION

Various admittance models of an open ended coaxial sensor have been proposed to determine complex permittivity of materials. These models include analytical models such as capacitance, admittance, virtual line and rational function models [1] as well as numerical techniques based on the finite element method, finite difference time domain method and method of moment.

Unfortunately, all the opened ended coaxial models require measured values of complex reflection coefficient to compute permittivity of the material under test. Recently, there has been

*Received 29 August 2012, Accepted 12 December 2012, Scheduled 2 January 2013*

* Corresponding author: Kim Yee Lee (kylee@utar.edu.my).

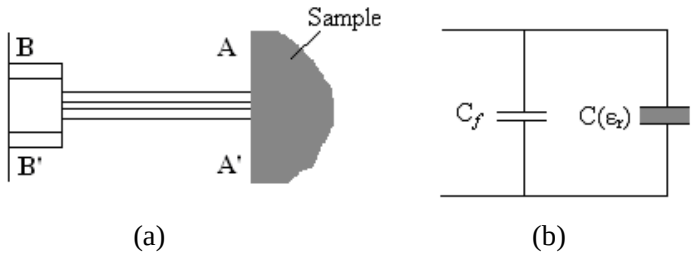


**Figure 1.** Open ended reflection method, (a) coaxial sensor terminated by a semi-infinite sample, and (b) capacitive equivalent circuit at plane $A$-$A'$.

an increasing demand for a simple equipment to determine complex permittivity of materials based on reflection measurements of open ended coaxial sensors [2–7].

This paper presents a dual open ended coaxial sensor system requiring only amplitude measurements of the reflection coefficients from two different open-ended coaxial sensors to calculate the complex permittivity of a sample. An improved capacitance model has been derived to calculate the complex reflection coefficient which in turn is used to determine the complex permittivity of a sample under test.

## 2. CAPACITANCE MODEL AND MODIFIED CAPACITANCE MODEL

The measurement configuration of the open-ended coaxial sensor and its capacitive equivalent circuit are illustrated in Figures 1(a) and (b), respectively [8]. In this model, the capacitance consists of two parts: $C(\varepsilon_r)$ which is related to the dielectric properties of the sample, and the fringing capacitance $C_f$ which is independent of dielectric properties of the sample.

The reflection coefficient, $\Gamma$, of the open ended coaxial sensor at $AA'$ plane is related to the characteristic impedance, $Z_0$, of the measurement system and the complex relative permittivity, $\varepsilon_r^*$, of the sample under test in the form

$$\Gamma^* = \Gamma e^{j\Phi} = \frac{1 - j\omega Z_0 \left[C(\varepsilon_r^*) + C_f\right]}{1 + j\omega Z_0 \left[C(\varepsilon_r^*) + C_f\right]} \tag{1}$$

where $C(\varepsilon_r^*) = C_0\varepsilon_r^*$, and $C_0$ is the capacitance of the capacitor filled with air, $C_f$ the capacitance independent of the material, and $\omega$ the operation angular frequency. The values of $C_0$ and $C_f$ are found by

calibrating the open ended sensor with a standard sample of known dielectric permittivity, such as deionized water [9].

Expanding the complex notation in Equation (1) gives:

$$\Gamma^* = \Gamma' + j\Gamma'' = \frac{1 - j\omega Z_0 \left[C_0(\varepsilon_r' + j\varepsilon_r'') + C_f\right]}{1 + j\omega Z_0 \left[C_0(\varepsilon_r' + j\varepsilon_r'') + C_f\right]} \tag{2}$$

where the real and imaginary parts of complex reflection coefficient, $\Gamma^*$, are expressed as:

$$\Gamma' = \frac{1 + \Gamma''\omega Z_0 C_0 \varepsilon_r' + \omega Z_0 C_0 \varepsilon_r'' + \Gamma''\omega Z_0 C_f}{1 - \omega Z_0 C_0 \varepsilon_r''} \tag{3}$$

$$\Gamma'' = \frac{(1 + \Gamma')(\omega Z_0 C_0 \varepsilon_r' + \omega Z_0 C_f)}{\omega Z_0 C_0 \varepsilon_r'' - 1}. \tag{4}$$

From Equation (2),

$$\varepsilon_r^* = \frac{1 - \Gamma^*}{j\omega Z_0 C_0 \left(1 + \Gamma^*\right)} - \frac{C_f}{C_0} \tag{5}$$

where the real and imaginary parts of $\varepsilon_r^*$ are respectively

$$\varepsilon_r' = \frac{-2\Gamma''}{\omega Z_0 C_0 \left(|\Gamma|^2 + 2\Gamma' + 1\right)} - \frac{C_f}{C_0} \tag{6}$$

$$\varepsilon_r'' = \frac{|\Gamma|^2 - 1}{\omega Z_0 C_0 \left(|\Gamma|^2 + 2\Gamma' + 1\right)} \tag{7}$$

By substituting Equations (6) and (7) into Equations (3) and (4), they can be represented as:

$$\Gamma' = \frac{|\Gamma|^2 - 1 - \omega Z_0 C_0 \varepsilon_r'' \left(1 + |\Gamma|^2\right)}{2\omega Z_0 C_0 \varepsilon_r''} \quad \text{(Real)} \tag{8}$$

$$\Gamma'' = \frac{(C_0\varepsilon_r' + C_f)\left(1 - |\Gamma|^2\right)}{2C_0\varepsilon_r''} \quad \text{(Imaginary)} \tag{9}$$

Equations (8) and (9) suggest that the real and imaginary parts of $\Gamma$ are amplitude dependent and independent of the phase of the reflection coefficient.

The fringing field capacitance $C_f$ is independent of the permittivity of material under tests $\varepsilon_r^*$. Assuming $C_f = 0$ and substituting Equations (8) and (9) into Equation (4) leads to

$$\frac{C_0\varepsilon_{app}'\left(1 - |\Gamma|^2\right)}{2C_0\varepsilon_{app}''} = \frac{\left(1 + \frac{|\Gamma|^2 - 1 - \omega Z_0 C_0 \varepsilon_{app}''\left(1 + |\Gamma|^2\right)}{2\omega Z_0 C_0 \varepsilon_{app}''}\right)\omega Z_0 C_0 \varepsilon_{app}'}{\omega Z_0 C_0 \varepsilon_{app}'' - 1} \tag{10}$$

$\varepsilon'_r$ and $\varepsilon''_r$ in Equation (4) are replaced with an apparent dielectric constant $\varepsilon'_{app}$ and loss factor $\varepsilon''_{app}$, respectively in Equation (10).

Rearranging Equation (10) in the form

$$\begin{aligned}&\left(2\omega Z_0C_0+2\omega Z_0C_0|\Gamma|^2\right)\varepsilon''_{app}+\left(\omega Z_0C_0-\omega Z_0C_0|\Gamma|^2\right)\left(\varepsilon'^2_{app}+\varepsilon''^2_{app}\right)\\&=\left(|\Gamma|^2-1\right)\end{aligned} \tag{11}$$

Allows matrix representation of two sets of measurement data

$$\begin{aligned}&\begin{bmatrix}2\omega Z_0C_{01}+2\omega Z_0C_{01}\,|\Gamma_1|^2 & \omega Z_0C_{01}-\omega Z_0C_{01}|\Gamma_1|^2\\ 2\omega Z_0C_{02}+2\omega Z_0C_{02}|\Gamma_2|^2 & \omega Z_0C_{02}-\omega Z_0C_{02}|\Gamma_2|^2\end{bmatrix}\begin{bmatrix}\varepsilon''_{app}\\ \varepsilon'^2_{app}\ +\varepsilon''^2_{app}\end{bmatrix}\\&=\begin{bmatrix}|\Gamma_1|^2-1\\ |\Gamma_2|^2-1\end{bmatrix}\end{aligned} \tag{12}$$

Leading to

$$\varepsilon''_{app}=\frac{\left(C_{02}^2-C_{01}^2\right)\left(|\Gamma_1|^2-1\right)\left(1-|\Gamma_2|^2\right)}{2\omega Z_0C_{02}C_{01}\left(C_{02}\left(1+|\Gamma_1|^2\right)\left(1-|\Gamma_2|^2\right)-C_{01}\left(1+|\Gamma_2|^2\right)\left(1-|\Gamma_1|^2\right)\right)} \tag{13}$$

And

$$\varepsilon'^2_{app}+\varepsilon''^2_{app}=\frac{C_{02}(|\Gamma_1|^2-1)(1+|\Gamma_2|^2)-C_{01}(|\Gamma_2|^2-1)(1+|\Gamma_1|^2)}{\omega^2Z_0^2C_{02}C_{01}(C_{01}(1-|\Gamma_1|^2)(1+|\Gamma_2|^2)-C_{02}(1-|\Gamma_2|^2)(1+|\Gamma_1|^2))} \tag{14}$$

where

$$\varepsilon'_{app}=\sqrt{\left(\varepsilon'_{app}\right)^2+\left(\varepsilon''_{app}\right)^2-\varepsilon''^2_{app}} \tag{15}$$

The real and imaginary parts of the complex reflection coefficient $\Gamma$ can now be calculated by replacing $\varepsilon''$ with $\varepsilon''_{app}$ and $\varepsilon''$ with $\varepsilon''_{app}$ in Equation (8) and Equation (9) respectively,

$$\Gamma' = \frac{|\Gamma|^2-1-\omega Z_0C_0\varepsilon''_{app}\left(1+|\Gamma|^2\right)}{2\omega Z_0C_0\varepsilon''_{app}} \quad \text{(Real)} \tag{16}$$

$$\Gamma'' = \frac{C_0\varepsilon'_{app}\left(1-|\Gamma|^2\right)}{2C_0\varepsilon''_{app}} \quad \text{(Imaginary)} \tag{17}$$

Hence both the real $\Gamma'$ and imaginary $\Gamma''$ parts of the reflection coefficient in Equations (16) and (17) can be calculated in conjunction with Equations (13) and (15) by measuring only the magnitudes $|\Gamma|^2$ of two different open ended coaxial sensors system.

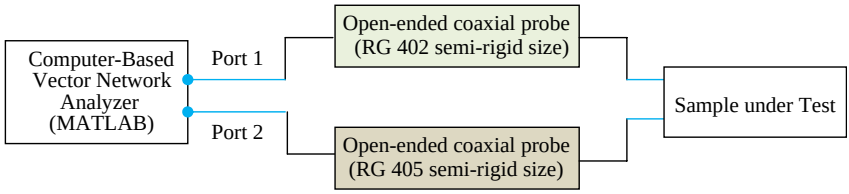


(a)

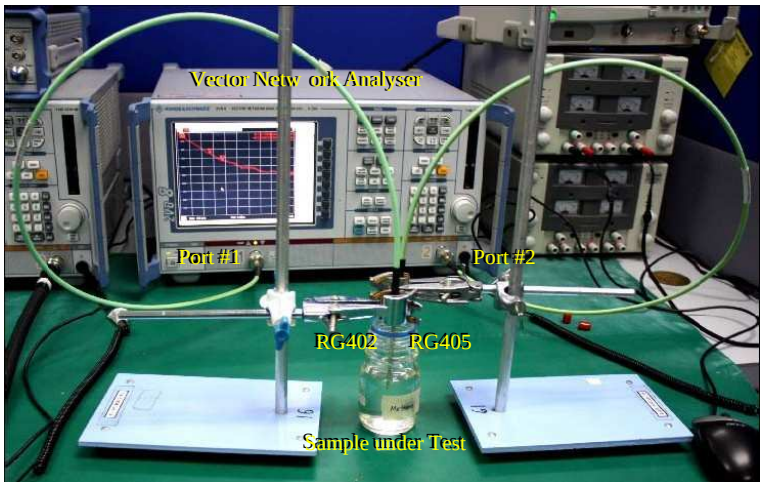


(b)


(c)

**Figure 2.** (a) Measurement block diagram. (b) Measurement setup. (c) RG402 and RG405 open ended coaxial sensors.

## 3. MEASUREMENT SYSTEM

The measurement setup shown in Figure 2 consists of a Rohde-Schwarz ZVA8 Vector Network analyzer (VNA) and two open ended coaxial sensors fabricated from commercial RG402 and RG405 semi-rigid

cables. The RG402 semi-rigid cable has inner and outer conductor radii $a = 0.4572\,\text{mm}$ and $b = 1.5113\,\text{mm}$, respectively. In contrast, the RG405 semi-rigid cable has smaller inner and outer conductor radii $a = 0.2552\,\text{mm}$ and $b = 0.8382\,\text{mm}$. The VNA was in default configuration setting with 201 points, 0 dBm, and CW mode. The VNA was connected to both sensors via two LL142 50 ohm 18 GHz low loss coaxial cables. The amplitude of the reflection coefficient, $|\Gamma_1|^2$ and $|\Gamma_2|^2$ for both the RG402 and RG405 coaxial sensors, respectively, were measured in the frequency range between 300 kHz and 8 GHz. All measurements were conducted in ambient temperature of 25°C. The minimum separation distance between the two sensors was kept more than half wavelength of the operating frequency to avoid coupling. Since it was difficult to calibrate at plane $A$-$A'$ of the sensor, the port extension technique was applied to extend the calibration plane to the reference plane. Both $|\Gamma_1|^2$ and $|\Gamma_2|^2$ were normalized values with respect to the unloaded sensor (i.e., without sample).

All data storage and computation were implemented in the computer-based VNA. The reflection coefficient magnitude and phase of the sample can be calculated from the measured magnitude $|\Gamma_1|^2$ and $|\Gamma_2|^2$ using Equations (16) and (17) in conjunction with Equations (13) and (15).

For calculation of complex permittivity, the capacitance model was used. Modified capacitance is used particularly for calculation of apparent permittivity ignoring the fringing field capacitance $C_f$. The modified capacitance model cannot be used because it will cause some error since $C_f$ is assumed to be zero. The calculated reflection coefficients in Equations (16) and (17) were then used to determine the permittivity of the sample under test using Equations (6) and (7). The values of $C_0 = 1.953\varepsilon_0(b-a)$ and $C_f = 0.0404\varepsilon_0(b-a)$ were used, where $b$ and $a$ are outer and inner radii of the open ended coaxial sensor.

For comparison purposes, a set of complex reflection coefficients was measured using VNA. The VNA was calibrated using standard two-port TRL calibration.

## 4. RESULTS AND DISCUSSIONS

The experimental and theoretical calculated reflection coefficients for both RG402 and RG405 type sensors were compared to VNA measurement results. Figures 3, 4 and 5 show the comparison for water, methanol and ethanol, respectively. Theoretical means calculated reflection coefficient of the sensor using Equations (16) and (17) by permittivity values obtained from Debye model [10, 11],

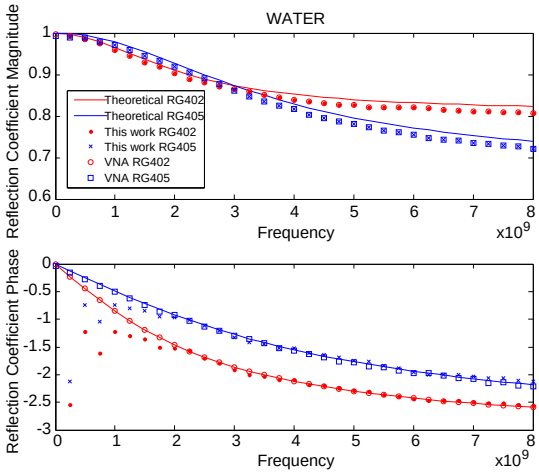


**Figure 3.** Reflection coefficient of water.

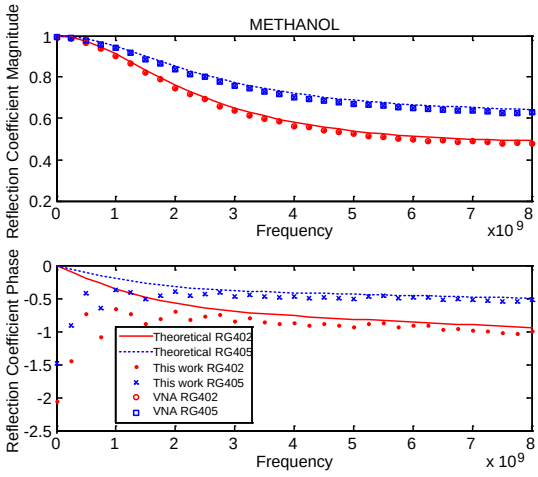


**Figure 4.** Reflection coefficient of methanol.

while experimental (this work) means calculated reflection coefficient obtained by Equations (16) and (17) using magnitude reflection coefficient measured by VNA. And VNA means the complex reflection coefficient measured by calibrated VNA. Magnitudes of the experimental result were exactly the same as the VNA result since both were measured by VNA. Theoretical calculated reflection coefficient magnitudes have a slight difference due to permittivity values obtained

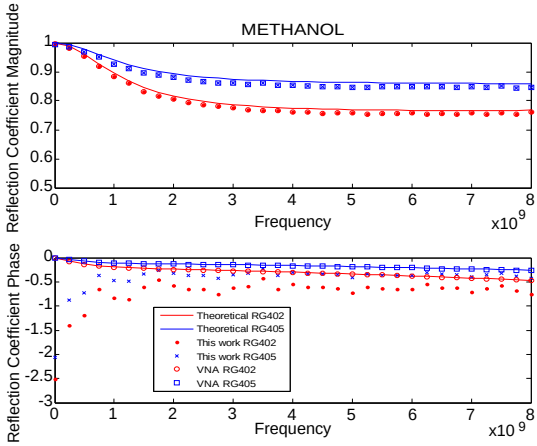


**Figure 5.** Reflection coefficient of ethanol.

from Debye model.

In Figure 3, theoretical calculated RG402 and RG405 sensors' results are in good agreement with VNA measurement results. Errors occurred in frequency less than 2 GHz for experimental results. The high deviation between the experimental and theoretical calculated reflection coefficient values at low frequencies was due to the limitation of Equations (16) and (17). In Equations (16) and (17), the changes in lower frequency are smaller and lead to difficulties in detecting reflection coefficient magnitude differences between two used sensors.

Figure 4 illustrates that for reflection coefficients phase of methanol there was good agreement between theoretical and VNA measurement results. Same error occurred for frequency less than 3 GHz in experimental results. The error of reflection coefficient phase decreases with increasing frequency for both RG402 and RG405 sensors.

Figure 5 illustrates reflection coefficients for ethanol. Good agreement between theoretical and VNA measured results is observed. The error of reflection coefficient phase decreases with increasing frequency. Similar to methanol in Figure 4, the reason for bigger error in ethanol measurement is that it has lower permittivity value compared to the methanol liquid. It can be clearly seen that the accuracy for reflection coefficient phase increases with increasing operation frequency and permittivity value.

The calculated complex reflection coefficient was used to determine the relative permittivity of sample by using Equations (6) and (7). It was in good agreement with Debye model for water

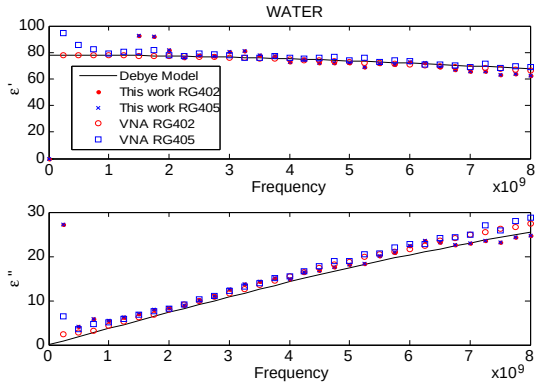


**Figure 6.** Theoretical and measurements permittivity of water.

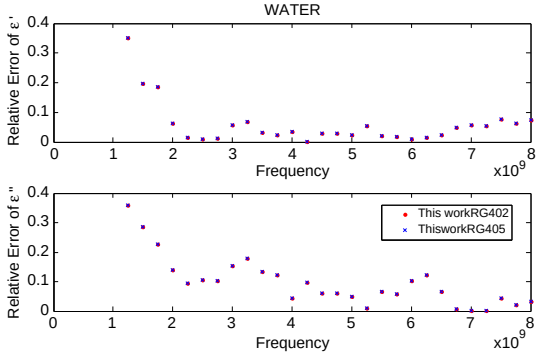


**Figure 7.** Error of water permittivity measurements.

measurement above 2 GHz as illustrated in Figure 6. The error at frequencies below 2 GHz is contributed by the error in reflection coefficient phase calculation as discuss previously.

After 2 GHz, the measured relative error of water permittivity $\varepsilon'$ (dielectric constant) and $\varepsilon''$ (loss tangent) are less than 0.1 and 0.2, respectively, as shown in Figure 7.

The measured complex permittivity of the methanol was in good agreement with Debye model and VNA measurements as illustrated in Figure 8. Both RG402 and RG405 coaxial sensors are able to perform accurate permittivity measurement for frequency more than 3 GHz.

The relative errors for frequency above 3 GHz are less than 0.25 and 0.1 for $\varepsilon'$ and $\varepsilon''$, respectively, as shown in Figure 9. The error decreases with increasing frequency.

The measured $\varepsilon'$ of the ethanol was slightly higher than VNA

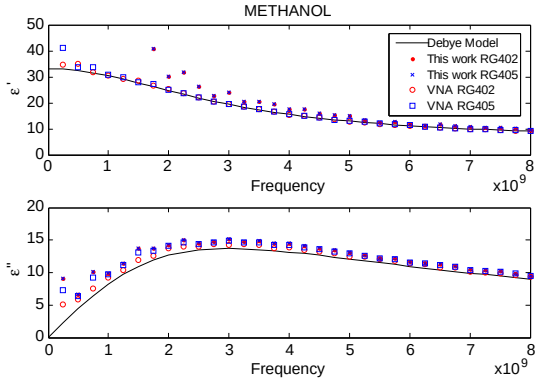


**Figure 8.** Theoretical and measurements permittivity of methanol.

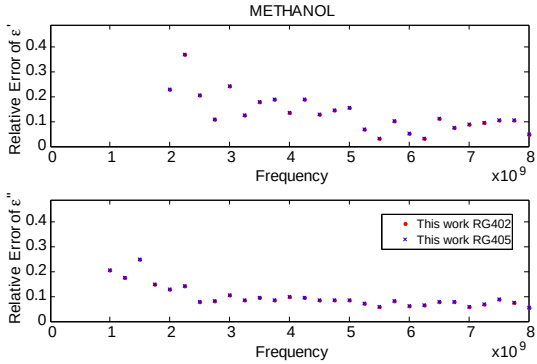


**Figure 9.** Error of methanol permittivity measurements.

measurement and Debye model for both RG402 and RG405 coaxial sensors as illustrated in Figure 10. The error decreases with increasing frequency. On the other hand, for measured $\varepsilon'$ of the ethanol there was good agreement between theoretical and VNA measured results. Both RG402 and RG405 are able to perform accurate $\varepsilon''$ measurement for frequency more than 3 GHz.

The relative errors for ethanol measurements are typically 1.50 and 0.15 for $\varepsilon'$ and $\varepsilon''$, respectively above 3 GHz as shown in Figure 11. The error slowly decreases with increasing frequency.

Overall, the relative error for $\varepsilon''$ remains low even the values of sample's permittivity are small. In contrast, the relative error in $\varepsilon'$ increases significantly when the permittivity of sample is decreased, which shows that the constraint of this method which is less accurate

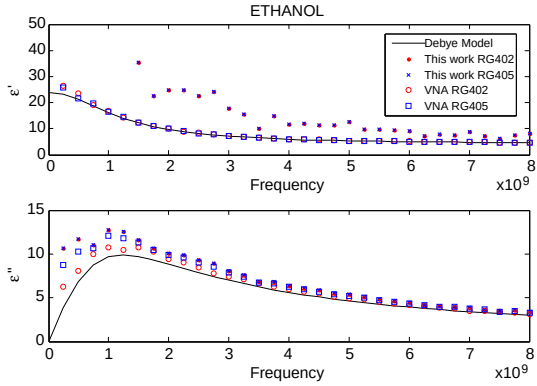


**Figure 10.** Theoretical and measurements permittivity of ethanol.

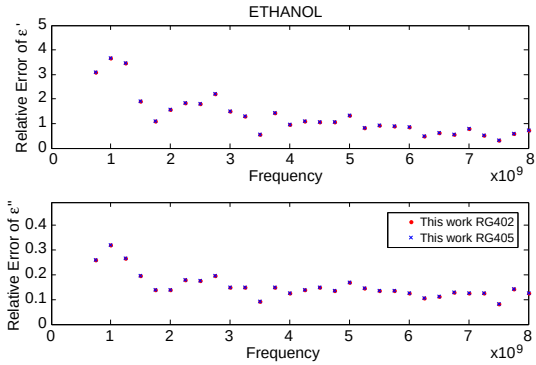


**Figure 11.** Error of ethanol permittivity measurements.

especially when the permittivity value of sample under test is low. The $\varepsilon'$ produces higher error than the $\varepsilon''$ due to higher accumulate errors from both $\Gamma'$ and $\Gamma''$ for dielectric constant calculation as in Equation (6). On the other hand, only $\Gamma''$ contributes to error for $\varepsilon''$ calculation as in Equation (7).

## 5. CONCLUSION

It is found that the suggested dual open-ended coaxial technique provides alternative method to determine complex reflection coefficient by using two magnitude measurements. It is also shown that one is able to determine permittivity of a sample using two magnitudes from two different sizes of open ended coaxial sensors. The proposed solution

is very attractive because of low cost and simple measuring devices. This method, due to large measurement error, is only useful for the measurements of liquids with high permittivity value or with water content above 50%.

## ACKNOWLEDGMENT

Authors wish to acknowledge the Universiti Tunku Abdul Rahman for the financial support through the UTAR Research Fund (UTARRF/C2-10/L3).

## REFERENCES

1. Berube, D. and F. M. Ghannouchi, "A comparative study of four open-ended coaxial sensor models for permittivity measurements of lossy dielectric/biological materials at microwave frequency," *IEEE Trans. Microwave Theory and Techniques*, Vol. 44, No. 10, 1928–1934, 1996.
2. Wang, Y. and M. N. Afsar, "Measurement of complex permittivity of liquids using waveguide techniques," *Progress In Electromagnetics Research*, Vol. 42, 131–142, 2003.
3. Sokoll, T. and A. F. Jacob, "In-situ moisture detection system with a vector network analyser," *Meas. Sci. Tech.*, Vol. 18, No. 4, 1088–1093, 2007.
4. Hasar, U. C., "Permittivity determination of fresh cement-based materials by an open-ended waveguide probe using amplitude-only measurements," *Progress In Electromagnetics Research*, Vol. 97, 27–43, 2009.
5. Hasar, U. C. and O. Simsek, "An accurate complex permittivity method for thin dielectric materials," *Progress In Electromagnetics Research*, Vol. 91, 123–138, 2009.
6. Lee, K. Y., Z. Abbas, Y. K. Yeow, M. D. Nur Sharizan, and C. E. Meng, "In situ measurements of complex permittivity and moisture content in oil palm fruit," *The European Physical Journal — Applied Physics,* Vol. 49, No. 3, 2010.
7. Chen, Q., K.-M. Huang, X. Yang, M. Luo, and H. Zhu, "An artificial nerve network realization in the measurement of material permittivity," *Progress In Electromagnetics Research*, Vol. 116, 347–361, 2011.
8. Gajda, G. and S. S. Stuchly, "An equivalent circuit of an open-ended coaxial line," *IEEE Trans. Instrum. Meas.*, Vol. 32, No. 4, 506–508, 1983.

9. Ghannouchi, F. M., R. G. Bosisio, Y. Demers, and R. Guay, "Computer aided measurement of dielectric properties of saline solutions using a six-port reflecometer," *IEEE Trans. Instrum. Meas.*, Vol. 38, No. 2, 505–508, 1989.
10. Kaatze, U., "Reference liquids for the calibration of dielectric sensors and measurement instrumentals," *Meas. Sci. Tech.*, Vol. 18, No. 4, 967–976, 2007.
11. Misra, D., M. Chabbra, B. R. Epstein, M. Mirotznik, and K. R. Foster, "Noninvasive electrical characterization of materials at microwave frequencies using an open-ended coaxial line: Test of an improved calibration technique," *IEEE Trans. Microwave Theory and Techniques*, Vol. 38, No. 1, 8–14, Jan. 1990.